RSC Advances

ROYAL SOCIETY OF CHEMISTRY

www.rsc.org/advances

Cite this: DOI: 10.1039/c0xx00000x

www.rsc.org/xxxxxx

ARTICLE TYPE

Exocyclic self-assembly behaviors of carboxylic acid and lariat ether macrocyclic hosts: regulation by pendent arm

Rong Guo, Wei Wang, Weiping Yang, Yuanyin Chen and Shuling Gong*

Received (in XXX, XXX) Xth XXXXXXXXX 20XX, Accepted Xth XXXXXXXXX 20XX

DOI: 10.1039/b000000x

Interaction of 1,4-dicarboxybenzene (PTA) with N,N'-disubstituented dibenzo-diaza-18-crown-6-ethers (**I, II, III, IV**) bearing flexibility side chain arms afforded the exocyclic supramolecular complexes of compositions **1** (**I**·PTA), **2** (**II**·PTA·0.2H2O), **3** (**III**·PTA) and **4** (**IV**·PTA), while with N-substituented dibenzo-aza-18-crown-6-ethers (**V, VI, VII**) afforded the endo-coordinated H_2O salts **5** [3(**V**·H2O)·(3PTA·7H_2O)], **6** [(**VI**· H_2O)·(PTA·3H_2O)] and **7** [2(**VII**· H_2O)· (PTA·11H_2O)], whose structures were determined by a single crystal X-ray method. These products were also obtained by the same synthetic conditions. Single crystal X-ray structural investigations on these solids confer: $P\bar{1}$ space symmetry for compound **III** and complexes **3, 5** and **7**; $C2/c$ space symmetry for the complexes **1, 2** and **4**; $P2_1/n$ space symmetry for compound **I**; $P2_12_12_1$ for complex **6**. The macrocyclic entities in compounds **I, III** and complexes **1, 2, 3, 4** with the 'chair-like' conformation of the crown ether ring and the extended arrangement of the pendant arms, adopt the structure as 'out-out' cyclic amines. But the macrocyclic entities in salts **5** and **6** adopt the C-shape conformation. The side chain arm may introduce minor crystal structure disparity, particularly 3D packing types in the exocyclic complexes **1, 2, 3** and **4**, while the arrangements of the pendant arms in protonated mono-sidearm crown ethers. Moreover, each complex with distinct ionic states, indicates that the proton transfer depends also upon the solid state environment.

Introduction

Crystal engineering is a powerful technique to reveal the role of various noncovalent interactions assembling molecules to crystal with desired structures and specific chemical/physical properties.[1] But the main impediments of designing and modifying noncovalently bound supramolecular structures are (i) the multiplicity of possible orientations of the molecules in crystals, (ii) the inaccuracies in estimating energies, and (iii) the entanglement of thermodynamic and kinetic contributions to crystal growth.[2] It has been recognized that limit the possible arrangement of the molecules in the solid state with respect to one another has been considered one of the most rational approaches to gain control over the arrangement of molecules in space, incorporation of a small number of functional groups.[2,3] Supramolecular synthon is a powerful concept for crystal engineering in the design of zero- to three-dimensional (0D to 3D) architectures.[4] Among the synthons, with robust and anisotropic nature, hydrogen-bonding (HB) synthons are quite useful in designing the low-dimensional supramolecular motifs.[5] Recently, HB synthons based on the carboxylic acid-amine complexes have drawn much attention from the crystal engineering community.[6] These groups are useful in various applications such as chiral synthesis[7] and separation,[8] supramolecular low-dimensional assemblies,[3, 9] and topological supramolecular chirality.[6c, 10] Supramolecular building blocks based on amines and carboxylic acids [5c, 11] offer good chemical diversity and provide a useful structural handle in its preference for 1D geometries. Besides, organic salts[12] and co-crystals[12a, 13] could be distinguished by the protonation-deprotonation behavior in carboxylic acid-amine complexes.[12a, 14] Both ionic hydrogen bonds in organic salts and hydrogen bonds in co-crystals have been investigated extensively. Furthermore, there are many works[15] proved that the competition hydrogen bond between different functional groups in forming particular intermolecular interactions definitely affects the predicability of a particular supramolecular synthon, influencing the design of supramolecular structures.

Aza-crown ether[16] is a well-known family of macrocyclic compounds[17] with important uses as a good coordination agent for a wide range of metals and cations. The anion complexation properties are similar to those in certain biological system due to their nitrogen lone pairs and N-H moieties. The uses of aza-crown ethers to form complexes with organic acids are also quite common.[18] As we know, unlike oxygen-bearing crown ethers, aza-bearing analogues have a tendency to show a repulsive interaction between adjacent nitrogen donors, the interaction leads to a *trans* (or *anti*) torsion arrangement, akin to the sulfur-containing macrocycles.[16a] Lee[19] concluded that the exocyclic coordination behavior in sulfur containing macrocycles may result from the repulsive interaction between adjacent sulfur donors. The strategy for macrocyclic ligand-based crystal engineering is to tune the structural and electronic features of a

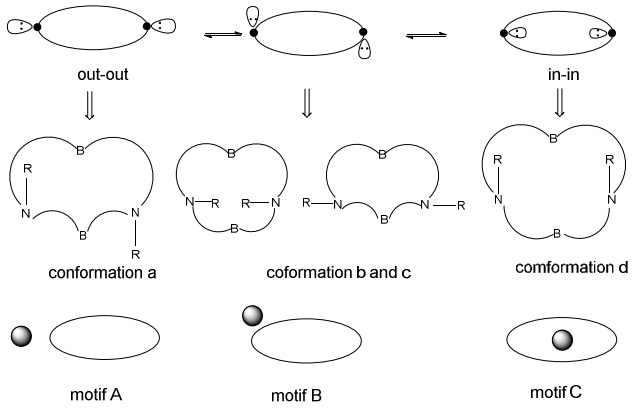

Scheme 1 The "out-in" designation referred to the orientation of the nitrogen lone pairs in diaza-crown ethers: out-out (left), in-in (right), conformation with axial positions of lone pairs (middle), and possible motifs of host-guest.

given macrocycle according to the guest. This should be practicable to prepare new molecular networks and materials based on aza-crown ether by controlling the orientation of the lone pair electrons on N atoms. The 'out-in' designation (Scheme 1), referring to the orientation of the nitrogen lone pairs relative to the interior or external in out-in bicyclic amines and cryptands proposed by Simmons,[20] would also be applied to aza-crown ethers. The interactions that attaching guests to the aza-crown ethers are head-to-face (HF),[16b, 16c, 17a, 17c, 17d, 21] head-to-edge (HE)[18] and head-to-head (HH), in which type (HE) and type (HF) have been experimentally verified by the supramolecular networking of macrocycles based on *exo* and *endo*-coordination. However, type (HH) in the diaza-18-crown-6 *exo*-coordination compounds is not fully explored yet. Fonari's studies[18a, 22] on lariat crowns and diaza-crown ethers showed both type (HE) and type (HF) with the flexibility macrocycle and rigidity pendant. In contrast with aliphatic crown ether, the stability constants of benzo-crown ethers are known to be lower, due to their higher rigidity and lower basicity of the oxygens caused by their conjugation with the aromatic ring.[17b] For this property, the conformations of the dibenzo-azacrown ether may be akin to the semi-rigid dibenzo-crown ether: C-shape[16b, 23] and S-shape.[24] Disparities between them could be caused by the various orientations of the lone pair electrons of N atoms and substituent groups. The relationship between the macrocyclic conformations and the orientations of the lone pair electrons in N atoms are shown in scheme 1.[25] According to this, the steric hindrance of substituent group on N atom would have influence in the orientation of the lone pair electrons for dibenzo-aza-18-crown-6 ethers. To investigate the influence of side chains on the host-guest chemistry based on azacrown ethers, we have chosen terephthalic acid (PTA) with linear functional topology and a series of semi-rigid macrocycles N,N'-disubstituented dibenzo-diaza-18-crown-6s (DBDA18C6) and N-substituented dibenzo-aza-18-crown-6s (DBA18C6) bearing flexibility substituent groups as the host (Scheme 2), resulting in applications such as molecular (or ion) sensing and exchange. The exocyclic head-to-edge or head-to-head arrangement of PTA as the robust supramolecular motif would be preserved in the crystals.

Whether proton transfer has occurred from acid to base as Childs[12b] noted, depends upon both the Δ*p*Ka value (*p*Ka of base

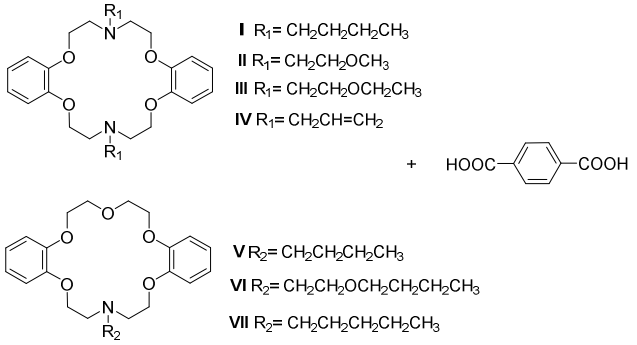

Scheme 2 Target 1,4-dicarboxybenzene and lariat ethers.

- *p*Ka of acid) and the crystalline environments. According to the studies by Nangia,[26] the transfer of proton is uncertain in the range $0 < \Delta pKa < 3.75$, but above 3.75 it is salt and below 0 it forms a neutral complex. For PTA (pKa_1 = 3.49, 25°C; pKa_2 = 4.46, 25°C) and azacrown ether (**I, II, III, IV, V, VI, VI** 7~8, 25°C predicted by SCI-finder), and this would be complicated with salts or co-crystals. But in solid, the nature (co-crystal/salt) of the complex is generally determined by the location of the H atom and the bond lengths of two C-O bond in carboxylic group. It has been elucidated that the two C-O bond distances are comparable ($\Delta D_{C-O} < 0.03$) for a carboxylate ion, whereas they are distinct ($\Delta D_{C-O} > 0.08$) for a neutral carboxyl group.[12b] IR spectra have been recorded, and look for disappearance of the bands due to COOH and appearance of the bands due to COO^- in the case of deprotonation and appearance of the bands due to NH^+, it is helpful to clarify whether protonation of amines occur or not.

For the first time, the structures of compounds (**I**, **III**) and the complexes of PTA with di-sidearm DBDA18C6s and mono-sidearm DBA18C6s in solid were isolated and characterized by X-ray single-crystal diffraction. In this paper, by choosing semi-rigid macrocycle and similiar side chain groups, we have shown that the pendant arms affect the supramolecular structure of complexes **1, 2, 3, 4, 5**, **6** and **7** in same crystallization medium and the different protonation-deprotonation behaviors by using X-ray single crystal diffraction and FT-IR spectra. Also in the discussion about the packing modes of the molecular crystals, it is important to understand non-covalent interactions such as the N-H···O, O-H···N, C-H···O hydrogen bondings [27] and C-H···π [28] or π···π stacking interactions [29], which play a critical role in controlling the packing modes of molecular crystals.

Results and discussion

Crystal structures of compound I and III.

Free macrocycle **I** crystallizes in the monoclinic space group $P2_1/n$ with half a molecule in the asymmetric unit. Crystal of macrocycle **III** is in a triclinic cell and structure solution, and was performed in the space group $P\bar{1}$, the asymmetric unit contains half of DBDA18C6 (**III)** molecule. The oxygen atoms in compounds **I** and **III** are arranged in an *endo*-dentate mode typical for most crowns.[17b] The 18-crown-6 molecule displays a 'chair-like' conformation in **I** and **III** (Fig. 1), two methylene groups on opposite sides of the ring are in *anti* conformation and are turned inward to fill the macrocyclic central void. The two

nitrogen atoms extend out in a *trans*-fashion with the pendent

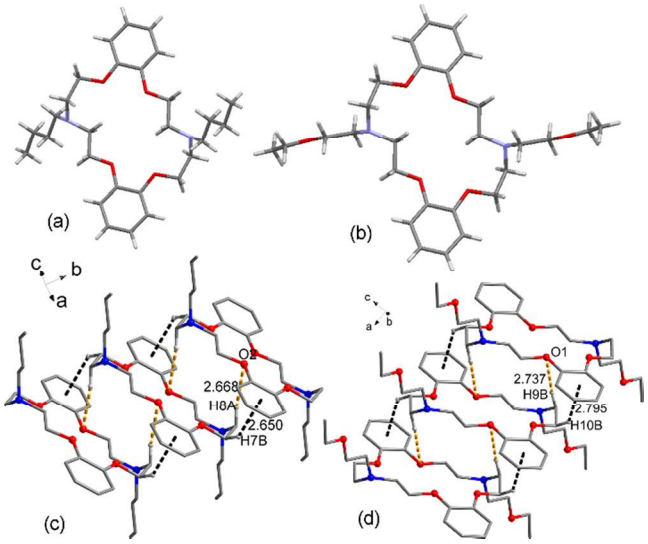

Fig. 1 (a) X-ray crystal structure of compound **I**; (b) X-ray crystal structure of compound **III**; (c) (d) fragment of crystal packing in **I** and **III** showing the association of the molecules in a ladder via C-H···π and C-H···O interactions.

arms in the axial position, apt to the 'out-out' conformation (Scheme 1). Obviously, Figure 1 shows lariat ethers **I** and **III** both in the extended conformation. These structures have not been report yet, show both difference from aliphatic azacrown ethers and dibenzo-crown ethers. As we know, the benzene may be present as a subcyclic unit that contributes no heteroatom to the macrocycle but does not otherwise alter the essential (O-C-C)n crown ether framework. This has obvious effects on the macrocyclic structure. First, replacement of OCH_2-$CH_2OCH_2CH_2O$ by OCH_2C-CH-CCH_2O rigidifies the macrocycle. Second, each replacement results in the loss of a donor group relative to diethyleneoxy.[17b] So, the semi-rigid feature of the macrocycle and the flexibility of the pendent arms can be explained for the structures of **I** and **III** in solid.

In compound **I**, along the *b* axis two uniform macrocycle stacks interacted *via* C-H···π interactions (C7-H7B···Cg(crown): H7B···Cg 2.65 Å, C7···Cg 3.468(3) Å, C7-H7B···Cg 140°) and C-H···O hydrogen bonding interactions (C8-H8A···O2: H···O= 2.668 Å, C···O= 3.578 Å, C-H···O= 152°, forming the ladder-like structure. And similar packing stacks along *c* axis in compound **III** (C10-H10B···Cg(crown): H10B···Cg= 2.79 Å, C10···Cg= 3.576(2) Å, C10-H10B···Cg= 138°; C9-H9B···O1: H···O= 2.737 Å, C···O= 3.659 Å, C-H···O= 159°). Generally the intermolecular interactions of C-H···O(OCH2) hydrogen bonding based the methoxy groups in the crown systems results in a stepwise packing structure. In the structures of compound **I** and **III**, the C-H···π interactions should also be beneficial to the packing, even more availably.

Crystal structure of complex 1 (I·PTA).

Single crystal of **1** was prepared in a monoclinic cell and structure solution was performed in the space group *C*2/*c*. The asymmetric unit of **1** was found to contain half moiety of PTA acid and DBDA18C6 (**I**). The structure is stabilized *via* O1-H1···N1 hydrogen bonds connecting *para*-hydroxyl group of PTA and the DBDA18C6 moiety molecule respectively (Fig. 2a). It is idiosyncratic for the PTA to attach with crown with head-to-head arrangement except head-to-face. Hydrogen bonding interactions [O1-H1···N1 = 1.77(2) Å; O1-H1···N1 = 172(5)°] involving the N of the DBDA18C6 and OH of the PTA moieties lead to the formation of 1D motif A (Scheme 1); the 1D linear ribbons are further packed in parallel fashion along *b* axis (Fig. 2b), form a staircase-like layer. Two layers of crystal packing of **1** are demonstrated in Fig. 2b with the C-H···π interactions [aromatic CH/π hydrogen bond C7-H7···Cg(crown): H7···Cg= 2.93 Å, C7···Cg= 3.751(3) Å, angle C7-H7···Cg= 146°. And C18-H18D···Cg(PTA) hydrogen bond: H18D···Cg= 3.24 Å, C18···Cg= 3.815(4) Å, angle C18-H18D···Cg= 119°].

Crystal structure of complex 2 (II·PTA·0.2H_2O).

The complex **2** crystallized in the monoclinic space group *C*2/*c*. The asymmetric portion of the unit cell contains 0.5 crown ether: 0.5 PTA. Hydrogen bonding interactions [O1-H1A···N1 = 1.74(2) Å; O1-H1A···N1 = 164(5)°] involving the OH of the PTA and N of the crown moieties lead to the formation of 1D motif A (Scheme **1**); along *b* axis, the 1D ribbons are further packed in parallel fashion *via* the C-H···O hydrogen bonding interactions (Fig. 2c). Lattice occluded water molecules are also observed within the bilayer structure stabilized by the water-carboxylate hydrogen bonding interactions (Fig. 3B 3b). The water molecules are bridging the two PTA molecular *via* the O6-H6A···O2 hydrogen bonding [O6-H6A···O2= 2.16 Å; O6-H6A···O2= 161.9°] with 2_1 symmetric arrangements along *c* axis (Fig. 3B). And it could be noted here that weak interactions such as C7-H7···π (aromatic CH/π hydrogen bond: H7···Cg= 2.81 Å, C7···Cg= 3.626(3) Å, C7-H7···Cg= 144°) and C17-H17A···π (H17A···Cg= 2.87 Å, C17···Cg= 3.532(9) Å, C17-H17A···Cg= 126°) also play a role in shaping the 3D supramolecular architectures in solid, similar to the complex **1**. And the TGA measurement (ESI: table S11) of complex **2** shows a weight loss of 0.60% in the temperature range 175-190°C, which corresponds to the loss of lattice water molecules (theoretical value of 0.56%).

Crystal structure of complex 3 (III·PTA).

Complex **3** crystallized in the centrosymmetric triclinic space group $P\bar{1}$. The asymmetric unit is composed of half of the DBDA18C6 moiety and PTA moiety. As elucidated in Fig. 4a, hydrogen bonding interactions [O1-H1B···N1= 1.71(6) Å; O1-H1B···N1= 176(5)°] involving the OH of the PTA and N of the crown moieties lead to the formation of 1D motif A (Scheme 1). Along *a* axis, the 1D linear ribbons are further packed parallelly by the C-H···O hydrogen bonding interactions (Fig. 2e), which form the 'inclined staircase' step. While the mutual arrangement of the layers are attributed to a 'staircase' packing motif where adjacent 'staircases' are arranged in parallel by the π···π interactions (Cg···Cg= 4.12 Å, perpendicular distance 3.56 Å) (ESI: Table S10b) between the benzenes of macrocycles in different layers. (Fig. 3C) While, the interlayer C(pendent arm)-H···π(PTA) hydrogen bonding interaction (C18-H18C···π: H18C···Cg= 3.11 Å, C18···Cg= 3.85 Å, C18-H18C···Cg= 133°) also can be found in complex **3**.

Crystal structure of complex 4 (IV·PTA).

The complex **4** crystallized in the monoclinic space group *C*2/*c*.

The asymmetric unit is composed of half of the DBDA18C6 moiety and PTA moiety. Hydrogen bonding interactions [O1-

Cite this: DOI: 10.1039/c0xx00000x

www.rsc.org/xxxxxx

ARTICLE TYPE

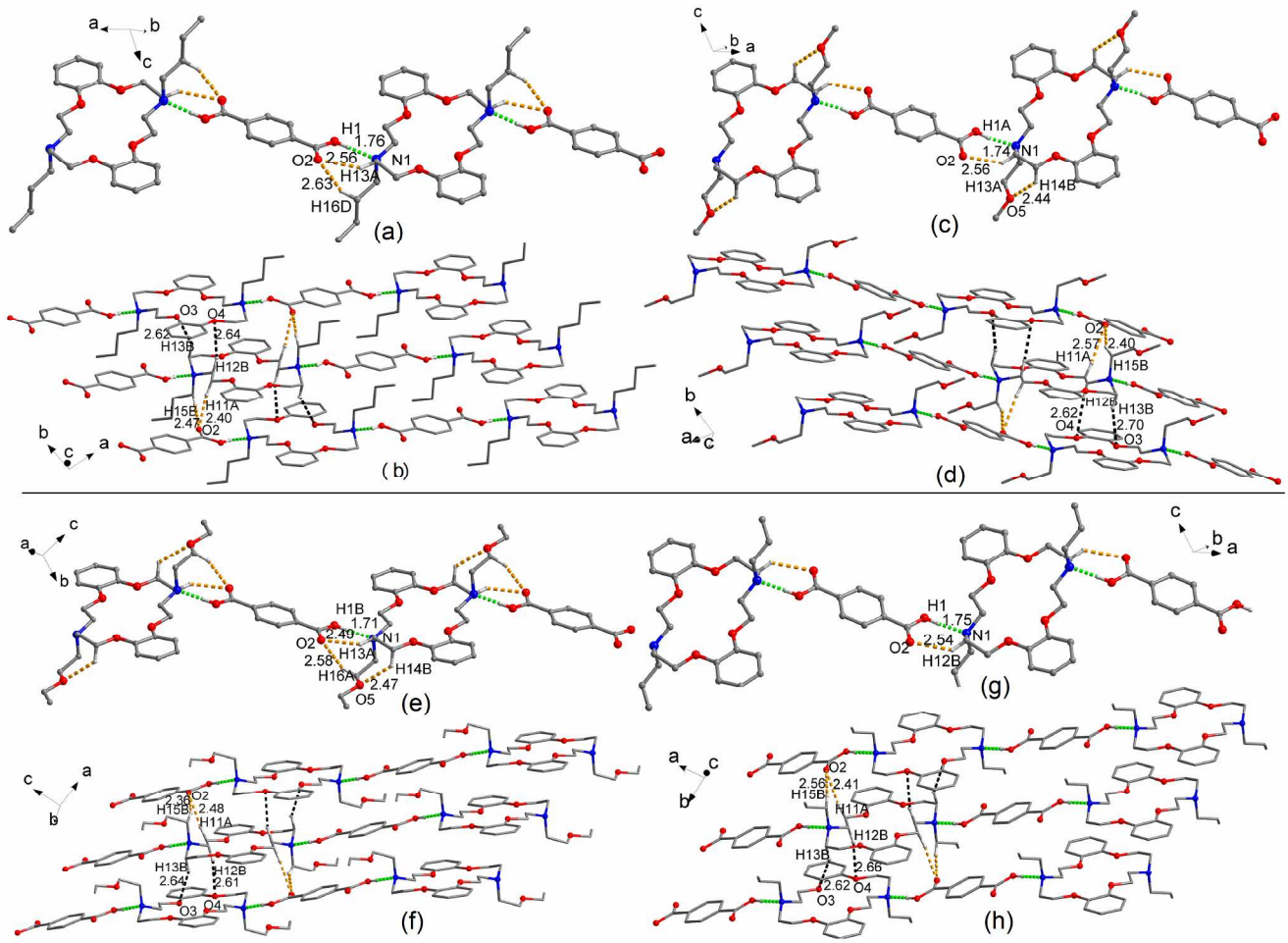

Fig. 2 Illustration of the single crystal structures of complex **1, 2, 3, 4**: (a) (c) (e) (g) Hydrogen bonding interactions forming 1D motif ; (b) (d) (h): parallel packing of the 1D networks along the *b* axis through C-H···O hydrogen bondings of complexes **1, 2, 4**, respectively.(broken line). (f) parallel packing of the 1D networks along the *a* axis through C-H···O hydrogen bondings of complex **3** (broken line).

H1 ···N1= 1.75(4) Å; O1-H1···N1= 177(4)°] involving the OH of the PTA and N of the crown moieties lead to the formation of 1D motif A (Scheme 1) suggesting a ribbon structure that is sandwiched between DBDA18C6·PTA units, the 1D linear ribbons are further packed in parallel fashion by the C-H···Ohydrogen bonding interactions (Fig. 2e, 2f). Interestingly, the 1-D linear ribbons build staircase-like columns *via* C-H···O (2.41 Å, 2.56 Å) hydrogen bond interactions between PTA and the side arm of the DBDA18C6 as well as weak C-H···O (2.62 Å, 2.66 Å) interactions between two parallel macrocycles. Layers are further packed by the C-H···π interactions [aromatic CH/π hydrogen bond C7-H7···Cg(crown): H7···Cg= 2.73 Å, C7···Cg= 3.542(3) Å, angle C7-H7···Cg= 144°. And C17-H17B···Cg(PTA) hydrogen bond: H17B···Cg= 3.27 Å, C17···Cg= 4.086(4) Å, angle C17-H17B···Cg= 145°] (Fig. 3D), the staircases are arranged in the herringbone-type packing.

Crystal structures of complex 5.

The complex **5** [3(**V**·H_2O)·(3PTA·7H_2O)] crystallizes in the triclinic space group $P\bar{1}$, has a layered structure containing water-crown ether inclusion. These waters are incorporated within the cavity of the protonated 18-crown-6 by N-H···O and O-H···O hydrogen bonds as shown in Figure 4. The asymmetric unit is comprised of three macrocyclic cations, three PTA anions, and ten water molecules. These water-crown ether inclusions are aggregated *via* C-H···π interactions, resulting in a chain. These chains are further connected into sheet through the π···π interactions (Cg···Cg= 4.57 Å, perpendicular distance 3.64 Å). Seated in the interlayer are seven water molecules and three PTA anions complexes that play a vital role in controlling the topology of the structures and also function in charge balancing. And hydrated anion layers are connected with crown ether layers *via* C-H (crown ether)···O(water) hydrogen bond [H17B···O18= 2.59 Å, C17B···O18= 3.577(5) Å, C17-H17B···O18= 173°]. The macrocycle adopt the distorted C-shape conformation, and the

Cite this: DOI: 10.1039/c0xx00000x

www.rsc.org/xxxxxx

ARTICLE TYPE

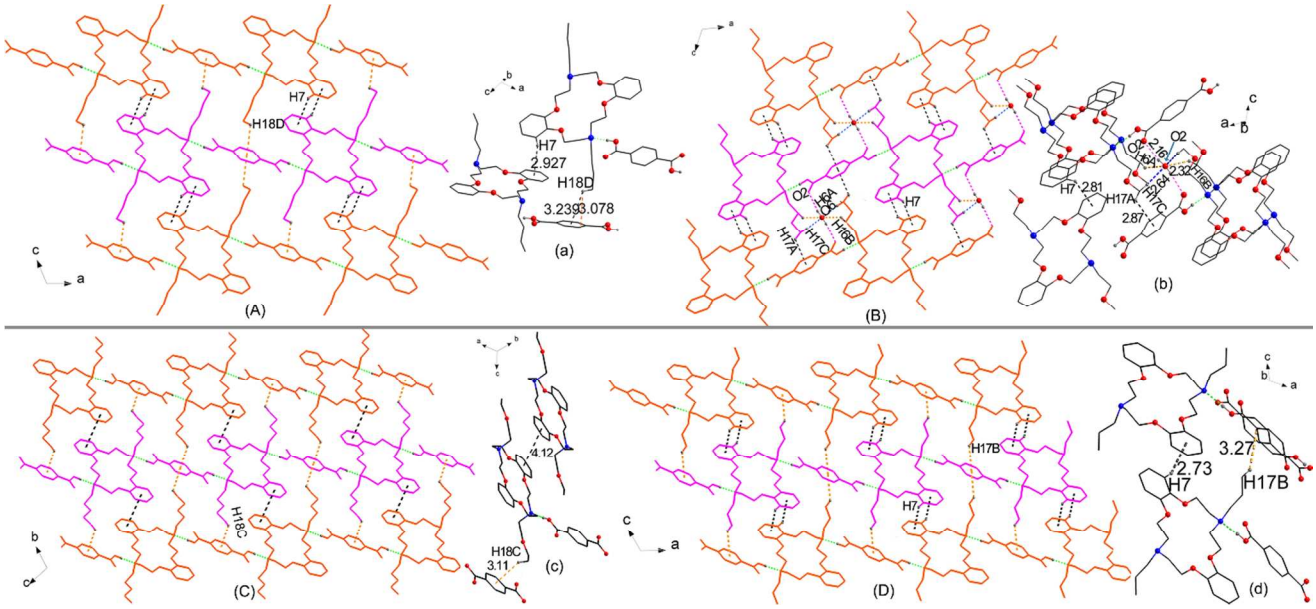

Fig.3 (A) The three-dimensional network of complex **1**. (B) The three-dimensional network of complex **2**. (C) The three-dimensional network of complex **3**. (D) The three-dimensional network of complex **4**. (a)(b)(c)(d) The details of the hydrogen bonding interactions between the layers for each complex. (macrocyles and PTA molecules in same sheet are with the same color in 3d structure).

pendent arm behind the macrocyclic back with the axial position. (Fig 4g)

Crystal structures of complex 6.

The complex **6** [(**VI**·H_2O)·(PTA·$3H_2O$)] crystallized in the orthorhombic space group $p2_12_12_1$ with one crown ether molecule, one PTA and ten H_2O molecules the asymmetric unit contains, has a layered structure. These layers of water-crown ether inclusions are less bent than in salt **5**. These waters are incorporated within the cavity of the protonated 18-crown-6 by N-H···O and O-H···O hydrogen bonds as shown in Figure 4. Two macrocycles are formed dimer *via* C-H···π interactions [C18A-H18B···π(phenylate): H···Cg= 2.59 Å, H-Perp= 2.56 Å, C-H···Cg= 144 Å; C18B-H18C···π(phenylate): H···Cg= 2.76 Å, H-Perp= 2.70 Å, C-H···Cg= 142 Å]. These crown ether dimers are further packed into sheet *via* C-H···π and C-H···O interactions. The interlayer space is filled with planar solvated PTA anion complexes as shown in Figure 4h. This is essential so that the overall charge balance is maintained. Meanwhile, the crown ether dimers are sandwiched between two solvated PTA anion layers *via* C-H···π and C-H···O interactions. Interestingly, the protonated macrocyle adopt the typical C-shape conformation similar to salt **5**, but the pendent arm in macrocycle front and with folded arrangement.

Crystal structures of complex 7.

The complex **7** [2(**VII**·H_2O)·(PTA·$11H_2O$)] with a 2:1 ratio, obtained from a 2:1 ratio of PTA and DBA18C6 (**VII**) from water/acetone, crystallizes in $P\bar{1}$ space group with two DBA18C6 (**VII**) and one PTA moieties in the asymmetric unit, has a layered structure containing water-crown ether inclusion. These waters are incorporated within the cavity of the protonated 18-crown-6 by N-H···O and O-H···O hydrogen bonds. These inclusions are aggregated *via* C-H···π interactions (aromatic interaction, T-shape), resulting in a 1D chain. (Fig. 4f) The chains are further connected through the C-H···O, C-H···π and π···π interactions into sheet (ESI: table S9, S10). In this 2:1 structure, both of the carboxyl groups of PTA is deprotonated. And hydrated anion layers are connected with cation crown ether layers *via* O-H(water)···O(crown), C-H(crown ether)···O(water), and C-H(crown ether)···O(PTA) hydrogen bonds. (Fig. 4i) The conformation of macrocycle and arrangement of pendent arm are similar to complex **5**.

Δp*K*a and the ionization state.

Studies on protonation-deprotonation behavior in carboxylic acid-amine complexes should be helpful in distinguishing if these complexes are salts or co-crystals.[30] The nature (co-crystal/salt) of the complex is generally determined by the location of the H atom and the bond lengths of two C-O bond in carboxylic group. The carbon-oxygen bond distances of the carboxylic group (Table 1) in *exo*cyclic complexes structures were not consistent with the deprotonated form (the C-O distances range within 1.240-1.278 Å). The evaluation can be also carried out by using FT-IR spectroscopy to observe O-H, N-H, and COOH signals and IR peak shifts due to hydrogen bonding.[12b, 31] When a salt is formed with amine bases, the carbonyl bands (IR bands) are shifted to lower frequencies by 30 to 40 cm^{-1}, but in cocrystals the

Cite this: DOI: 10.1039/c0xx00000x

www.rsc.org/xxxxxx

ARTICLE TYPE

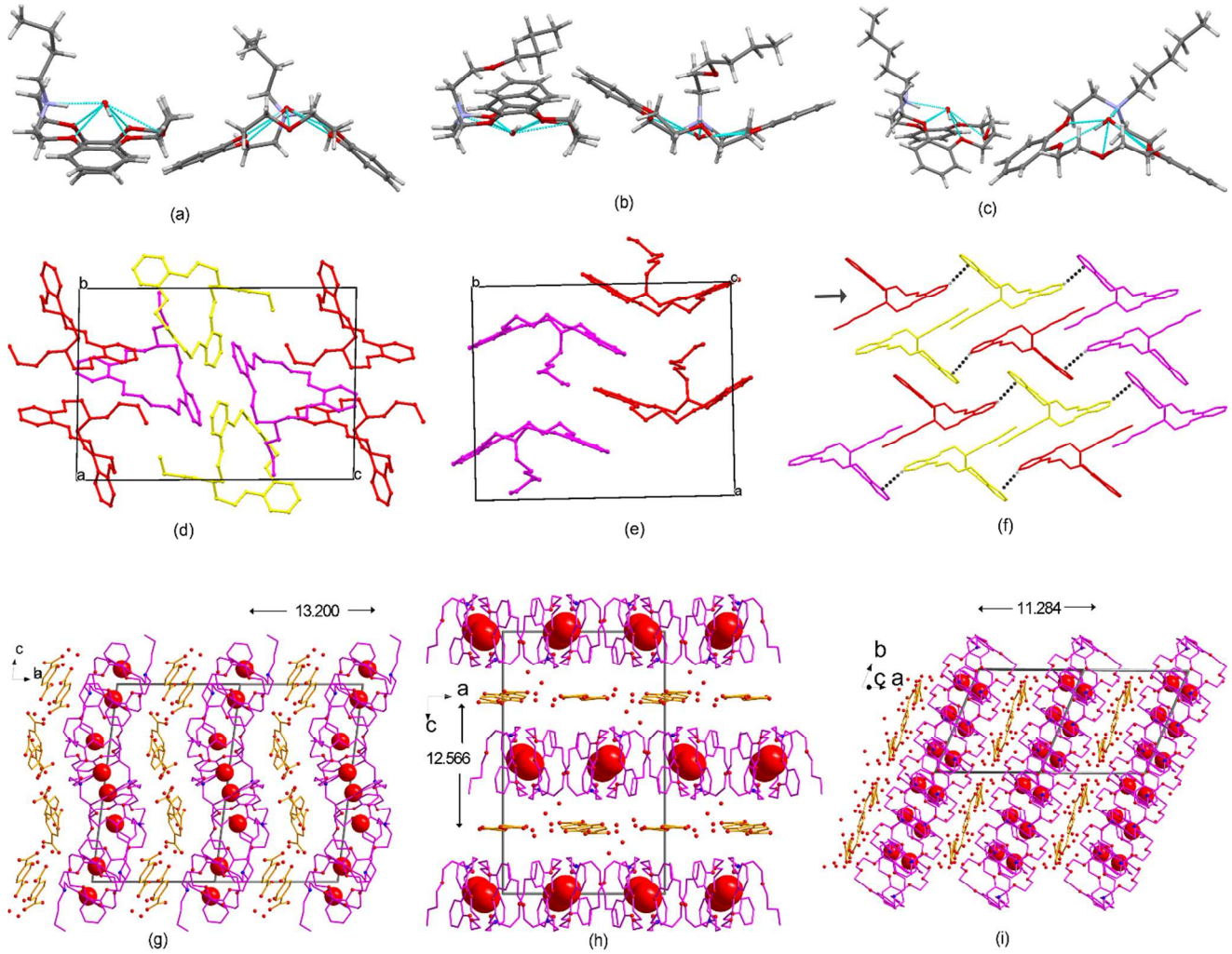

Fig. 4 Illustration of the single crystal structures of salts **5, 6** and **7**: (a) (b) (c)conformation of mono-sidearm crown ethers in each salt; (d) (e) (f) the structure of crown ether sheet in each salt, respectively.(g) (h) (i) the layer structures of each salt. (in 3d structure: magenta: crown ether; yellow: PTA; and red spacefill: the water in cavity, hydrogen atoms are omitted in sheet and. view directions of 3D layered structure: (g) [-1,1,0];(h) [0,1,0]; (i) [-1,0,1]).

carbonyls are shifted due to hydrogen bonding, the magnitude of the shift is relatively small (about 10 to 20 cm^{-1}). The IR data for complexes **1, 2, 3** reported here indicates that each is the presence of ~1645 cm^{-1} (COO^{-}), ~2750 cm^{-1} (NH^{+}) and of ~1685 cm^{-1} (COOH) indicating that partially deprotonation of the acid moiety, but for complex **4** is presence of 1687 cm^{-1} ,and absence of 1645 cm^{-1}, ~2750 cm^{-1} (figure S1 and S2). And the Fourier difference maps revealed that the acidic protons are partially positioned in proximity to the N-atom of the aza-crown ether molecule in exocyclic complexes **1, 2, 3**. The correlation between IR data and the nature of crown ether complexes is evident where both IR and single-crystal diffraction data exist. So the complexes **1, 2, 3** were classified as partially proton-transfer complexes, while there is no obvious proton transfer in **4** co-crystal. So in figures of exocyclic complexes **1, 2, 3** and **4**, we draw O-H···N hydrogen bonds. But all of the mono-sidearm DBA18C6s in complexes **5, 6** and **7** are totally protonated. Hence under the same crystallization condition, macrocycle bearing different structure or number of pendant arm with similar p*K*a, show different ionization properties. This indicate that the proton transfer depends also upon the solid state environment.

Exocyclic assembly behaviors by di-sidearm DBDA18C6s.

Obviously, in compound **I**, **III** and complexes **1, 2, 3** and **4**, the oxygen atoms in the crown are arranged in an *endo*-dentate mode typical for most crowns.[17b] In the exocyclic complexes **1, 2, 3** and **4**, similar to the compound **I** and **III** the two nitrogen atoms extend out in a trans-fashion, deviating from the phenylate plane (C5/C6/C7/C8/C9/C10/O3/O4b) at ±0.579 Å, ±0.697 Å, ±0.659 Å, ±0.442 Å for **1, 2, 3, 4** respectively. From the torsion angles (Table S1), we can see that the phenylate plane

Table 1 C-O bond lengths of the PTAs and the $\Delta D_{C\text{-}O}$ in complexes **1, 2, 3** and **4**.

Structure no.	$D_{C\text{-}O}$(short) Å	$D_{C\text{-}O}$(long) Å	$\Delta D_{C\text{-}O}$ Å
1	1.221	1.315	0.094
2	1.224	1.299	0.075
3	1.224	1.297	0.073
4	1.221	1.312	0.091

(C5/C6/C7/C8/C9/C10/O3/O4b) of the crown and one CH_2 unit (C11) are almost located on the same plane reference as plane R, in line with the specialty of semi-rigid macrocyle. Two phenylate planes in one macrocyle are not really in the same plane but in parallel in fact, and show less perpendicular distance through comparing the structures of compounds **I**, **III** and complexes **1**, **3** respectively. The planar PTA molecule is inclined at an angle of 9.11(6)°, 15.27(7)°, 12.73(6)°, 17.75(8)° to the mean plane R for **1**, **2**, **3**, **4**. So the di-sidearm macrocycles adopt the chair-shape conformation and the side arms with the axial position, similar to the structures of free macrocycle **I** and **III**. Consequently the crowns adopt a typical 'parallelogram' conformation[17a] (two phenylate planes in parallel) and nitrogen atoms in the macrocycle adopt an *exo*-orientation of the nitrogen lone pairs relative to the exterior by the torsions table, moreover two inversion-related methylene hydrogens turned inward toward the center of the ring. Obviously, the PTA with its hydrogen atom is involved in O-H···N hydrogen bonding by head-to-head type that result in the *exo*cyclic 1D structures like linear ribbon. Further, two methylene moieties in the macrocycle turn towards O-C group of the PTA with their hydrogen atom being involved in C-H···O hydrogen bonding with the PTA. Thus synthon A (Fig. 5), assembled by O1(carboxyl)-H···N1(DBDA18C6) and C(DBDA18C6)-H···O2(carbonyl) hydrogen bonds, controls supramolecular assembly in the crystal structures of PTA and N,N'-disubstituented DBDA18C6s. In exocyclic complexes **1**, **2**, **3** and **4**, PTA molecule attached to the crown group with head-to-head type, providing the *exo*-cyclic structures as motif A except motif B. There is poor information about the motif A of the aza-crown ethers and guest in solid. Motif B have been illustrated[15d, 16] by the aza-crown ethers bearing the phenolic side arms with acids.

Motif **B** have been shown in aza-crown ethers with the flexible macrocycle and rigid pendent arms that is resulting from steric effects,[18a, 22] *anomeric* effects[32] and hybrid method. However, in di-sidearm DBDA18C6s the *anomeric* effect must be resulting in the side arm with the axial position as the torsions of the crown rings.[33] Thus, the motif A effect could be resulting in the side arm *with* the axial position as the torsions of the crown rings.[33] And, the motif A in our work may be due to the orientation of the nitrogen lone pairs and the semi-rigidity of the DBDA18C6 ring as well as the flexibility of pendent arms as mentioned above. While the conformations of the asymmetric part of the pendant arms have turned out differently, for **I** : *trans*, *trans* and **III** : *trans*, *trans, trans;* **1** : *trans*, *trans* and **2** : g*uacha, trans*; for **3**: *guacha, trans, trans* and for **4** : *trans* (all beginning from N1 atom). It seems that the C14(macrocycle)-H···O5(pendent arm) intramolecular hydrogen bonding in complexes **2** and **3** can account for this disparities.

The 1D motif A ribbons are packed in parallel fashion along *b* axis in complexes **1**, **2**, **4** and *a* axis in **3** like 'inclined staircase' packing motif. It is unambiguous that the weak intermolecular C-H···O hydrogen bonds, which consists of two parts: C(pendent arm)-H···O-C(PTA) and C(macrocycle)-H···O(macrocycle), controlling the arrangement along *b* axis in **1**, **2**, **4** and *a* axis in **3** providing synthon B (Fig. 5). For **2** the distance of C13-H13B···O4# is 2.702 Å > 2.5 Å, instead of the strong O6-H6A···O2 ($d_{H...O}$= 2.16 Å) hydrogen bonding interaction exist (Fig. 2). Thus, the synthon B would also benefit from the pendent arms with the axial position.

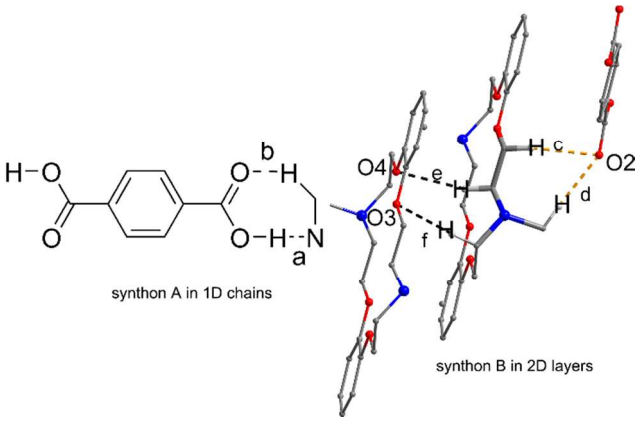

Fig. 5 The hydrogen bond synthons that appear in exocyclic complexes **1**, **2, 3** and **4**. (a: O1-H···N1, b: C13-H13A···O2, c: C11-H11A···O2#, d: C15-H15B···O2#, e: C12-H12B···O4#, f: C13-H13B···O3#)

Furthermore, 2D layers of crystal would pack to 3D network. As shown in Fig. 3, different 3D packing structures could be formed together with the weak π···π (offset, face-to-face) or CH···π (point-to-face) interaction, caused by the different pendent arms. The "competition" between different functional groups in forming particular intermolecular interactions influence the 3D packing structures. The mutual arrangement of the layers of complex **3** may be attributed to a 'staircase' packing motif where adjacent 'staircases' are arranged in parallel, which caused by the π···π (offset face-to-face) stacking. However, in the complexes **1**, **2, 4** and compound **I** the staircases are arranged in the herringbone-type packing due to the aromatic C-H···π (T-shape) interactions. Generally, as for the benzene dimers, geometry a (aromatic CH/π hydrogen bond; but this is often referred to as the point-to-face or T-shape aromatic interaction) is more favorable than geometry b (offset π/π stacking), though slightly (Fig. 6). Curiously, the crystal structures of **2** and **3** elucidate obvious disparities, for another neither aromatic CH/π hydrogen bond nor π···π (offset, face-to-face) interaction have been found in compound **III**. Thus, the structure of the pendant arms further affect the supramolecular structure based on N,N'-disubstituented DBDA18C6 bearing the pendent arms. And with the length of pendent arm less than five carbon atoms, di-sidearm DBDA18C6s in the crystal lattice apt to arrange in the herringbone-type packing through the aromatic CH/π hydrogen bonding (T-shape). Meanwhile, no proof in these crystals show that the constitution of pendent arm in di-sidearm DBDA18C6s affect the 3D packing structure.

In addition, the interlayer C(pendent arm)-H···π(PTA) hydrogen bonding interactions between pendent and PTA in **2** and **4** are stronger than in **1** and **3**, as the perpendicular distances of H to ring plane are different (**1**, 3.08 Å; **2**, 2.83 Å; **3**, 3.09 Å; and **4**,

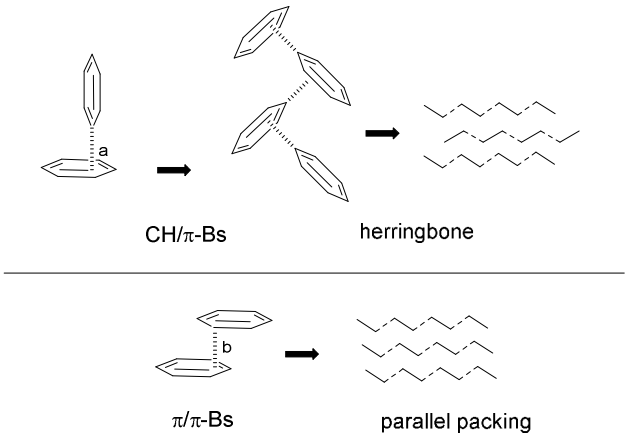

Fig. 6 Arrangement of crown ethers in the crystal lattice of compound **I** and complexes **1, 2, 4** through the aromatic CH···π (point-to-face, T-shape) interactions between the adjacent layers (top). The weak π···π (offset, face-to-face) interactions between the adjacent layers in complex **3**, causing a parallel packing arrangement (bottom).

2.82 Å). The reason maybe that the C(pendent arm)-H···O5 (water) hydrogen bondings make the pendent arm chain more curled in crystal structure **2** favoring suitable length to form C (pendent arm)-H···π(PTA) hydrogen bonds as well as in solid state **4**. Unfortunately, under the same conditions, we could not get the similar exocyclic complexes with longer pendent arms as PTA precipitate out first (R = $CH_2CH_2OCH_2CH_2CH_2CH_3$, $CH_2CH_2OCH_2CH_2OCH_2CH_2CH_2CH_3$).

Endo-coordinated water salts by mono-sidearm DBA18C6s.

Due to the hydrogen bondings with the water molecule in the cavity of the crown ether in salts **5**, **6** and **7**, the oxygen atoms and nitrogen atom in the crown are both arranged in an *endo*-dentate mode, and the macrocyclic entities adopt the C-shape conformations.[17b] The pattern observed here shows similar layered structure in salts **5, 6** and **7** with the sheet of protonated crown ether inclusions are sandwiched between solvated PTA anion layers. Interactions between the solvated PTA anion layers and crown ethers are all through C-H···O hydrogen bonging in salts **5**, **6** and **7**, but additional aromatic CH/π hydrogen bongings in salt **6**, O-H(water)···O hydrogen bongings in salt **7**. The structures of salts **5**, **6** and **7**, indicate that, in these solids the supramolecular self-assembly of the ion pairs is not governed by strong and directional hydrogen-bonding interactions as well as stronger and not so-directional electrostatic interactions between the cations and anions, reveal significant differences with exocyclic complexes **1**, **2**, **3** and **4**. The observations are consistent with the fact that the "competition" between different functional groups in forming particular intermolecular interactions influence the design of supramolecular structures. It may be noted here that the each packing of the protonated crown ethers are not identical in salts **5**, **6** and **7**, even resulting to a similar cationic sheet. In this sheet, salt **5** shows reasonable C-H(ethyleneoxy units)···π and π···π interactions. And salt **6** shows C-H(ethyleneoxy units)···π without π···π interactions. While, salt **7** shows aromatic CH/π hydrogen bonds and π···π interaction as well as C-H···O hydrogen bonds.

The pendent arm are bonding to the bridge N atoms with the axial position in the structure of salts **5**, **6** and **7**, however the arrangements of the pendent arms are in the opposite direction between salts **5, 6** with salt **7**.(Fig 4) The reasons of inconsistent results in salt **6** may be the N-H···O intramolecular hydrogen bond between the sidearm with protonated crown ether [N1A-H1A···O6A= 2.873(6) Å, N1B-H1B···O6B= 2.894(6) Å] as well as the conformation with smaller steric hindrance in the crystal structure. As we mentioned above, with longer pendent arms (R=$CH_2CH_2OCH_2CH_2CH_2CH_3$), the crystal of PTA with di-sidearm DBDA18C6 could not be obtained, but salt **6** have been obtained. These indicate that these side arms are flexible with the position depend upon the solid state environment, on the other hand the structure of the sidearm also affect the crystal structure.

Along with the diverse types of PTA-azacrown ether interactions, the complexes discussed herein demonstrate the different mutual arrangement of the components, which changes from the sidearm conformation in the cyclic heteroatoms and skeleton of macrocycle until the practically different arrangement. This observation demonstrate the remarkable reliability of the N···O interaction between the cyclic amines and aromatic carboxylates and the promising potential for design of multiple component crystals on the base of such interactions. Meanwhile, the pendant arms affect the supramolecular structure of aza-crown ether with acid: exocyclic structure by di-sidearm DBDA18C6s but endo-coordinated water salts by mono-side arm DBA18C6s.

Conclusions

X-ray studies for the exocyclic behaviors by N,N'-disubstituented dibenzo-diaza-crown ethers, but endo-coordinated water structures by N-substituted dibenzo-aza-crown ethers with same conditions, reveal that the importance of direct strong hydrogen bonging interaction and no-direct weak hydrogen bondings in the supramolecular self-assembly. The head-to-head arrangement of 1,4-dicarboxybenzene via O-H···N hydrogen bonding as the robust supramolecular motif is preserved in the *exo*cyclic supramolecular structures by the 'out-out' di-sidearm DBDA18C6s. But a series of layered structures were obtained by mono-sidearm DBA18C6s, with the sheet of protonated crown ether inclusions are sandwiched between solvated PTA anion layers and self-assembly of the ion pairs is not governed by strong and directional hydrogen-bonding interactions as well as stronger and not so-directional electrostatic interactions between the cations and anions. Moreover, the length of side chain arm may introduce minor crystal structure disparity in di-sidearm crown ether complexes, particularly 3D packing types with herringbone-type *via* aromatic CH/π hydrogen bond in complexes **1**, **2**, **4,** but parallel packing in complex **3**. The conformations of mono-sidearm crown ether in the salts **5**, **6** and **7** were influenced by the side chain chemical composition and molecular structure more than the side chain length.

The ionization states of carboxylic acid-DBDA18C6 complexes are different correspondingly, and the protonation-deprotonation behaviors in complexes **1, 2, 3** and co-crystal **4** are clear with the single-crystal X-ray diffraction analyses and FT-IR data. Furthermore, the assembly behaviors on these lariat ether may also be affected by the guests, and these are also currently under investigation.

Experimental

Crystallization.

The azacrown ethers (**I**, **II**, **III**, **IV**, **V**, **VI**, **VII**) were prepared according to the literature method.[16a, 16b] Single crystals were grown from CH_2Cl_2/hexane mixtures for compounds **I**, **II**, **III**, **IV**, while only crystals of compounds **I** and **III** are available. Azacrown ethers (**I**, **II**, **III**, **IV**, **V**, **VI**) and PTA in 1:1 (acid:amine) molar ratio in water/acetone medium, but **VII** and PTA in 2:1. The resultant mixture was subjected to reflux for two hours to ensure the homogeneous mixing of the two components. A colorless precipitate was obtained after complete removal of solvent by rotavapor. Single crystals were grown from water/acetone mixtures (25 mg of complexes in 4 mL solvents in 10 mL beaker) by slow evaporation at room temperature. Typically X-ray quality crystals were appeared after a few weeks.

IR Spectroscopy. Transmission infrared spectra of the solids were obtained using a Fourier-transform infrared spectrometer (Nicolet NEXUS670). 16 scans were collected at 4 cm^{-1} resolution for each sample. The spectra were measured over the range of 4000-400 cm^{-1}.

X-Ray crystallography.

X-Ray data of the crystals were collected on a Bruker D8 Quest CMOS single-crystal diffractometer with graphite filtered Mo-Ka (λ= 0.71073 Å) radiation. Data collections for crystals of **I**, **1**, **2**, **3**, **4**, **5**, **6** and **7** were carried out at 173(2)K and **III** at 298(2)K. The structures were solved by direct methods using the SHELXS-97[34] program and refined by Fullmatrix least-squares on F^2 using SHELXL97.[34] H atoms attached to O and N parents were found in the Fourier maps and refined with distance restraints, and referring to complex **1**, **2**, **3**, these H atoms were refined with a split atom model for the discussion of the behaviour on proton-transfer. Diagrams and publication material were generated using WinGX,[35] ORTEP,[36] and PLATON.[37] Crystallographic data and structural correction parameters are listed in Table 2.

Acknowledgements

We are grateful to the National Natural Science Foundation of China (20772092) and the Hubei Province Natural Science Fund for Distinguished Young Scholars (2007ABB021) for financial support.

Notes and references

College of Chemistry and Molecular Sciences, Wuhan University, Wuhan, 430072, PR China. E-mail: gongsl@whu.edu.cn; Fax: +86 27 68754067; Tel: +86 27 68752701.

† Electronic supplementary information (ESI) available: Table S1, S2: torsion angles of macrocyclic rings and the pendant arms; Table S3–S9: hydrogen bonds of supramolecular complexes **1**-**7**; Table S10a: CH···π hydrogen bonds, Table S10b: π·· π interactions. Table S11: TGA and DSC. Table S12 (figure S1, S2): FT-IR data. Crystallographic information file (cif). CCDC reference numbers 1048852–1048855, 1058279, 1058280, 1060647-1060649. For ESI and crystallographic data in CIF or other electronic format see DOI: 10.1039/c0xx00000x

1. G. R. Desiraju, *Nature*, 2001, **412**, 397-400.
2. J. C. MacDonald and G. M. Whitesides, *Chem Rev*, 1994, **94**, 2383-2420.
3. A. Ballabh, D. R. Trivedi and P. Dastidar, *Cryst Growth Des*, 2005, **5**, 1545-1553.
4. (a) G. R. Desiraju, *Angew. Chem. Int. Ed. in English*, 1995, **34**, 2311-2327; (b) P. Ganguly and G. R. Desiraju, *CrystEngComm*, 2010, **12**, 817-833; (c) A. Mukherjee, S. Tothadi and G. R. Desiraju, *Acc Chem Res*, 2014, **47**, 2514-2524.
5. (a) L. J. Prins, D. N. Reinhoudt and P. Timmerman, *Angew Chem Int Ed*, 2001, **40**, 2382-2426; (b) K. Sada, T. Tani and S. Shinkai, *Synlett*, 2006, **2006**, 2364-2374; (c) Y. Li, W. Yang, R. Guo, Y. Chen and S. Gong, *CrystEngComm*, 2012, **14**, 1455-1462.
6. (a) P. Sahoo and P. Dastidar, *Cryst Growth Des*, 2012, **12**, 5917-5924; (b) A. Lemmerer, *CrystEngComm*, 2011, **13**, 2849; (c) I. Hisaki, T. Sasaki, N. Tohnai and M. Miyata, *Chemistry*, 2012, **18**, 10066-10073.
7. A. Tanaka, K. Inoue, I. Hisaki, N. Tohnai, M. Miyata and A. Matsumoto, *Angewandte Chemie*, 2006, **118**, 4248-4251.
8. (a) K. Megumi, F. Nadiah Binti Mohd Arif, S. Matsumoto and M. Akazome, *Cryst Growth Des*, 2012, **12**, 5680-5685; (b) A. Ichikawa, H. Ono, T. Echigo and Y. Mikata, *CrystEngComm*, 2011, **13**, 4536-4548.
9. (a) A. D. Bond, *Cryst Growth Des*, 2005, **5**, 755-771; (b) L. Chen, H. Y. Zhang and Y. Liu, *J Org Chem*, 2012, **77**, 9766-9773; (c) Y. Liu and Y. Chen, *Acc Chem Res*, 2006, **39**, 681-691.
10. (a) T. Yuge, T. Sakai, N. Kai, I. Hisaki, M. Miyata and N. Tohnai, *Chemistry*, 2008, **14**, 2984-2993; (b) T. Sasaki, Y. Ida, A. Tanaka, I. Hisaki, N. Tohnai and M. Miyata, *CrystEngComm*, 2013, **15**, 8237.
11. (a) X. Li, S.-L. Gong, W.-P. Yang, Y.-Y. Chen and X.-G. Meng, *Tetrahedron*, 2008, **64**, 6230-6237; (b) Y. Li, W. Yang, Y. Chen and S. Gong, *CrystEngComm*, 2011, **13**, 259-268.
12. (a) S. Y. Han and H. Bin Oh, *Chem Phys Lett*, 2006, **432**, 269-274; (b) S. L. Childs, G. P. Stahly and A. Park, *Mol Pharmaceutics*, 2007, **4**, 323-338; (c) S. Bhattacharya and B. K. Saha, *Cryst Growth Des*, 2011, **11**, 2194-2204.
13. (a) R. Kaur, S. S. R. R. Perumal, A. J. Bhattacharyya, S. Yashonath and T. N. Guru Row, *Cryst Growth Des*, 2014, **14**, 423-426; (b) S. Kohmoto, S. Sekizawa, S. Hisamatsu, H. Masu, M. Takahashi and K. Kishikawa, *Cryst Growth Des*, 2014, **14**, 2209-2217.
14. (a) N. Stanley, V. Sethuraman, P. T. Muthiah, P. Luger and M. Weber, *Cryst Growth Des*, 2002, **2**, 631-635; (b) X.-C. Su, H.-K. Lin, S.-R. Zhu, L.-H. Weng, X.-B. Leng and Y.-T. Chen, *Supramol Chem*, 2002, **14**, 41-45; (c) S. B. Raj, N. Stanley, P. T. Muthiah, G. Bocelli, R. Ollá and A. Cantoni, *Cryst Growth Des*, 2003, **3**, 567-571; (d) X.-L. Zhang and X.-M. Chen, *Cryst Growth Des*, 2005, **5**, 617-622.
15. (a) B. Sarma and B. Saikia, *CrystEngComm*, 2014, **16**, 4753; (b) J. B. Nanubolu, B. Sridhar, K. Ravikumar, K. D. Sawant, T. A. Naik, L. N. Patkar, S. Cherukuvada and B. Sreedhar, *CrystEngComm*, 2013, **15**, 4448; (c) R. Montis and M. B. Hursthouse, *CrystEngComm*, 2012, **14**, 7466; (d) S. Ghosh, P. P. Bag and C. M. Reddy, *Cryst Growth Des*, 2011, **11**, 3489-3503.
16. (a) V. J. Gatto and G. W. Gokel, *J Am Chem Soc*, 1984, **106**, 8240-8244; (b) N. G. Lukyanenko, S. S. Basok and L. K. Filonova, *Journal of the Chemical Society, Perkin Transactions 1*, 1988, DOI: 10.1039/p19880003141, 3141; (c) V. Rüdiger, H.-J. Schneider, V. P. Solov'ev, V. P. Kazachenko and O. A. Raevsky, *Eur J Org Chem*, 1999, **1999**, 1847-1856; (d) P. Wei, X. Yan and F. Huang, *Chem Soc Rev*, 2015, **44**, 815-832; (e) S. Dong, B. Zheng, F. Wang and F. Huang, *Acc Chem Res*, 2014, **47**, 1982-1994; (f) Y. Gao, R.-L. Zhong, H.-L. Xu, S.-L. Sun and Z.-M. Su, *RSC Adv.*, 2015, **5**, 30107-30119; (g) D. Liu, T. Pang, K. Ma, W. Jiang and X. Bao, *RSC Adv.*, 2014, **4**, 2563-2567.
17. (a) G. W. Gokel, L. J. Barbour, R. Ferdani and J. Hu, *Acc Chem Res*, 2002, **35**, 878-886; (b) G. W. Gokel, W. M. Leevy and M. E. Weber, *Chem Rev*, 2004, **104**, 2723-2750; (c) S. J. Pond, O. Tsutsumi, M. Rumi, O. Kwon, E. Zojer, J. L. Bredas, S. R. Marder and J. W. Perry, *J Am Chem Soc*, 2004, **126**, 9291-9306; (d) E. Kleinpeter and A. Holzberger, *Tetrahedron*, 2006, **62**, 10237-10247; (e) H. Tomiyasu, J.-L. Zhao, X.-L. Ni, X. Zeng, M. R. J. Elsegood, B. Jones, C. Redshaw, S. J. Teat and T. Yamato, *RSC Adv.*, 2015, **5**, 14747-14755; (f) H.-L. Lee, N. Dhenadhayalan and K.-C. Lin, *RSC Adv.*, 2015, **5**, 4926-4933; (g) N. Gutowska, P. Seliger, G. Andrijewski, M. Siwy, M. Małecka and J. Kusz, *RSC Adv.*, 2015, **5**, 38435-38442; (h) X. Bao, D. Liu, Y. Jin, X. Liu and W. Jiang, *RSC Advances*, 2013, **3**, 6783; (i) M. Sarma, T. Chatterjee and S. K. Das, *RSC Advances*, 2012, **2**, 3920.
18. (a) M. S. Fonari, E. V. Ganin, S. S. Basok, K. A. Lyssenko, M. J. Zaworotko and V. C. Kravtsov, *Cryst Growth Des*, 2010, **10**, 5210-

5220; (b) J. M. Cole, P. G. Waddell and D. Jayatilaka, *Cryst Growth Des*, 2012, **12**, 2277-2287.
19. S. Park, S. Y. Lee, K. M. Park and S. S. Lee, *Acc Chem Res*, 2012, **45**, 391-403.
20. H. E. Simmons and C. H. Park, *J Am Chem Soc*, 1968, **90**, 2428-2429.
21. D. J. Wolstenholme, P. Sirsch, L. Onut, J. Flogeras, A. Decken and G. S. McGrady, *Dalton Trans*, 2011, **40**, 8301.
22. M. S. Fonari, E. V. Ganin, Y. M. Chumakov, M. M. Botoshansky, K. Suwinska, S. S. Basok and Y. A. Simonov, *New J Chem*, 2009, **33**, 1646.
23. J.-C. Aguilar, S. Bernès, P. Gómez-Tagle, R. A. Bartsch and J. de Gyves, *J Chem Crystallogr*, 2006, **36**, 473-479.
24. J. E. Beves, B. A. Blight, C. J. Campbell, D. A. Leigh and R. T. McBurney, *Angew Chem Int Ed*, 2011, **50**, 9260-9327.
25. M. B. Duriska, S. M. Neville and S. R. Batten, *Chem Commun (Camb)*, 2009, 5579-5581.
26. B. R. Bhogala, P. Vishweshwar and A. Nangia, *Cryst Growth Des*, 2005, **5**, 1271-1281.
27. (a) E. Arunan, G. R. Desiraju, R. A. Klein, J. Sadlej, S. Scheiner, I. Alkorta, D. C. Clary, R. H. Crabtree, J. J. Dannenberg, P. Hobza, H. G. Kjaergaard, A. C. Legon, B. Mennucci and D. J. Nesbitt, *Pure Appl Chem*, 2011, **83**; (b) G. R. Desiraju, *Acc Chem Res*, 1991, **24**, 290-296.
28. (a) S. Tsuzuki, *Annual Reports Section "C" (Physical Chemistry)*, 2012, **108**, 69; (b) M. Nishio, *Phys Chem Chem Phys*, 2011, **13**, 13873.
29. (a) C. A. Hunter and J. K. M. Sanders, *J Am Chem Soc*, 1990, **112**, 5525-5534; (b) C. Janiak, *J. Chem. Soc., Dalton Trans.*, 2000, 3885-3896; (c) R. R. Choudhury and R. Chitra, *CrystEngComm*, 2010, **12**, 2113.
30. (a) V. R. Hathwar, R. Pal and T. N. Guru Row, *Cryst Growth Des*, 2010, **10**, 3306-3310; (b) T. R. Shattock, K. K. Arora, P. Vishweshwar and M. J. Zaworotko, *Cryst Growth Des*, 2008, **8**, 4533-4545; (c) S. Mohamed, D. A. Tocher, M. Vickers, P. G. Karamertzanis and S. L. Price, *Cryst Growth Des*, 2009, **9**, 2881-2889; (d) B. Sarma, N. K. Nath, B. R. Bhogala and A. Nangia, *Cryst Growth Des*, 2009, **9**, 1546-1557.
31. C. B. Aakeroy, J. Desper and M. E. Fasulo, *CrystEngComm*, 2006, **8**, 586-588.
32. G. R. J. Thatcher, *The Anomeric Effect and Associated Stereoelectronic Effects*, American Chemical Society, Washington, 1993.
33. M. W. Hosseini, A. J. Blacker and J. M. Lehn, *J Am Chem Soc*, 1990, **112**, 3896-3904.
34. (a) G. M. Sheldrick, *Acta Crystallogr A*, 2008, **64**, 112-122; (b) G. M. Sheldrick, *SHELXL-97, A Program for Crystal Structure Solution*, University of Göttingen, Germany, 1997; (c) G. M. Sheldrick, *SHELXL-97, A Program for Crystal Structure Refinement*, University of Göttingen, Germany, 1997.
35. L. J. Farrugia, *J Appl Crystallogr*, 1999, **32**, 837-838.
36. L. J. Farrugia, *J Appl Crystallogr*, 1997, **30**, 565-565.
37. A. L. Spek, *J Appl Crystallogr*, 2003, **36**, 7-13.

Table 2 Crystallographic data and structure correction parameters.

Compound reference	**I**	**III**	**1**	**2**	**3**	**4**	**5**	**6**	**7**
CCDC number	1058279	1058280	1048852	1048853	1048854	1048855	1060647	1060648	1060647
Chemical formula	$C_{28}H_{42}N_2O_4$	$C_{28}H_{42}N_2O_6$	$C_{28}H_{42}N_2O_4$ •$C_8H_6O_4$	$C_{26}H_{38}N_2O_6$ •$C_8H_6O_4$ •0.2(H_2O)	$C_{28}H_{42}N_2O_6$ •$C_8H_6O_4$	$C_{26}H_{34}N_2O_4$ •$C_8H_6O_4$	3($C_{24}H_{34}NO_5$)• 3($C_8H_5O_4$)• 10(H_2O)	$C_{26}H_{37}NO_6$• $C_8H_5O_4$• 4(H_2O)	2($C_{25}H_{36}NO_5$) • $C_8H_4O_4$• 13(H_2O)
Formula Mass	470.64	502.64	636.76	644.31	668.76	604.68	1925.09	697.76	1259.42
Crystal system	Monoclinic	Triclinic	Monoclinic	Monoclinic	Triclinic	Monoclinic	Triclinic	Orthorhombic	Triclinic
a/Å	16.1140(18)	4.8922(15)	31.850(3)	31.427(4)	5.7584(5)	31.022(6)	15.5676(9)	15.4985(8)	12.9024(13)
b/Å	4.7953(5)	10.102(3)	5.7811(5)	5.8115(8)	10.5829(9)	5.8603(15)	16.2241(8)	18.7452(11)	12.9804(16)
c/Å	17.101(2)	14.454(4)	20.098(2)	19.863(2)	14.5837(13)	19.725(4)	21.6195(13)	25.1312(15)	31.537(4)
α/°	90.00	81.084(5)	90.00	90.00	103.242(3)	90.00	85.854(2)	90.00	82.392(4)
β/°	97.747(4)	87.770(5)	112.557(3)	114.729(4)	95.682(3)	118.646(6)	82.127(2)	90.00	82.392(4)
γ/°	90.00	84.859(5)	90.00	90.00	100.938(3)	90.00	66.1610(10)	90.00	82.392(4)
Unit cell volume/Å^3	1309.3(3)	702.7(4)	3417.4(6)	3295.2(7)	839.90(13)	3146.9(12)	4946.6(5)	7301.2(7)	4861.4(10)
Temperature/K	173(2)	298(2)	173(2)	173(2)	173(2)	173(2)	173(2)	173(2)	173(2)
Space group	*P2(1)/n*	*P*$\bar{1}$	*C2/c*	*C2/c*	*P*$\bar{1}$	*C2/c*	*P*$\bar{1}$	*P2(1)2(1)2(1)*	*P*$\bar{1}$
No. of formula units per unit cell, *Z*	2	1	4	4	1	4	2	8	3
No. of reflections measured	6253	4942	9043	7854	6796	10964	38605	33278	39452
No. of independent reflections	2273	2446	3090	2938	2988	2841	17369	7735	16713
R_{int}	0.0749	0.0448	0.0468	0.0750	0.0514	0.0845	0.0974	0.0920	0.1183
Final R_1 values ($I > 2\sigma(I)$)	0.0563	0.0552	0.0475	0.0519	0.0509	0.0513	0.0622	0.0569	0.0872
Final $wR(F^2)$ values ($I > 2\sigma(I)$)	0.1144	0.1683	0.1129	0.0888	0.1029	0.1244	0.0920	0.1307	0.1376
Final R_1 values (all data)	0.1226	0.0687	0.0932	0.1305	0.1091	0.1144	0.1714	0.1388	0.2170
Final $wR(F^2)$ values (all data)	0.1406	0.1827	0.1364	0.1113	0.1221	0.1816	0.1187	0.1702	0.1778